ORIGINAL PAPER

Spontaneous fracture of growing precipitates with large misfit strain

P. Ståhle · R. N. Singh · S. Banerjee

Abstract Precipitates that form as a result of phase transformation are studied with regard to mechanical behaviour and initiation of internal cracks. The focus is on precipitates occupying a larger volume than the surrounding matrix. Further the study is restricted to precipitates growing by incorporating material transformed from being matrix material to the phase of the precipitate. The phase transformation is here treated as a simple homogeneous swelling. The classical solutions for expanding inclusions predict that the inclusion becomes subjected to a constant homogeneous hydrostatic compression. During the process analysed here, added transformed material progressively relieve the compressive stress in the interior of the precipitate. As the process continues the stresses change from compression to tension in both radial and tangential directions in the centre of the precipitate. Further, growth of cracks in precipitates with poor fracture mechanical properties are studied. To simplify the analysis it is assumed that the fracture toughness is insignificant. The prediction is that around a third of the precipitate will fracture. The presence of a crack only has an insignificant effect on the load exerted by the swelling precipitate on the matrix.

1 Introduction

Diffusive transport of matter driven by gradients in temperature, electric potential, mechanical stress etc. may form precipitates. In metals the matter could be small molecules and electrons. Common molecules would be hydrogen atoms forming metal hydrides that are formed when the concentration of hydrogen becomes supercritical. Altered crystal structure and/or chemical conditions are usual causes of phase transformation. The process is generally accompanied by a change of the material volume leading to mechanical stress in the precipitate and its neighbourhood. Further, it is generally anticipated that the stress field affects the flux of matter, leaving a problem for coupled mechanics, heat transfer, diffusion etc.

Certain aspects of fracture were analysed on a larger length scale, thus avoiding the detailed stress distribution in and around the precipitates. In Grange et al. (2000) a Gurson material model was modified to capture the effect of present hydride precipitates on

P. Ståhle (✉)
Division of Solid Mechanics, Lund Institute of Technology,
22100 Lund, Sweden
e-mail: pers@solid.lth.se

R. N. Singh
Division of Materials Science, Malmö University,
20506 Malmö, Sweden

R. N. Singh · S. Banerjee
Mechanical Metallurgy Section, Materials Group,
Bhabha Atomic Research Centre, Mumbai 400085, India

the fracture properties. A somewhat more detailed model of zirconium and zirconium-hydride system, by Matvienko (2004), utilized a cohesive zone crack tip model where a fracture stress of the precipitates where incorporated as a reduction of the cohesive stress. The analysis predicts the fracture toughness and measured results, (Simpson and Cann 1979). Both the theoretical work and experiments show that the zirconium hydride is very brittle as fracture occurs at only a few MPa$\sqrt{\text{m}}$.

Well known classical work give exact solutions for swelling spherical, elliptic and cylindrical inclusions. Solutions for elastic-plastic material behaviour were established for spherical and cylindrical geometry, (Hill et al. 1947; Hill 1950; Taylor 1948). Later a solution for an elliptic geometry and elastic material a was given, (Eshelby 1957). A characteristic of the solutions, for deeply embedded inclusions, is that the solution predicts that the inclusion is subjected to pure hydrostatic stress. The analyses are, however, limited to simultaneous swelling in the entire inclusion, such as that caused by temperature change and differences in thermal expansion or phase transformation that occur simultaneously in the entire inclusion. Cases of progressive phase transformation have been analysed, using the classical models, cf. Leitch and Puls (1992), Leitch and Shi (1996), Singh et al. (2008b), Singh and Ståhle (2006). The solution gives an accurate description of the mechanical state in the matrix but it does not at all reflect the mechanical state of the precipitate state. The Eshelby solution was used by several to interpret the influence of accommodation energy on hydrogen solid solubility and hysteresis effects, (Puls 1990, 1984; Shi 1999; Singh et al. 2004).

Observations of micro cracking inside hydrides formed in a zirconium, zirconium hydride system cannot be explained by the solutions (Eshelby 1957; Hill 1950). Figure 1 shows central cracks in a blister formation induced by a temperature gradient away from a cold spot on the surface of a zirconium Zr–2.5 Nb pressure tube, (Singh 2009). The blister shaped precipitate is a zirconium hydride that expands linearly more than 6% during the stress free phase transformation. The cracks are present in a region that according to the solution (Hill 1950) should be subjected to compression and, thus, their appearance may be surprising. An attempt to simulate a more realistic phase transformation process using a finite element method and adding new material to the precipitate was made by Singh et al. (2008a).
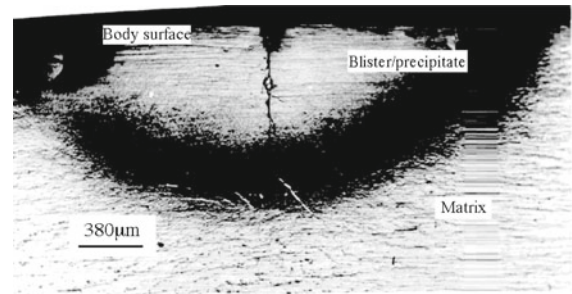

Fig. 1 Optical micrograph of hydride blister section, grown at a cooled spot in Zr–2.5 wt% Nb pressure tube material. A negative temperature gradient drags hydrogen towards the cold spot. At a critical concentration the new phase is formed. A crack is observed to traverse the central part of the blister

In this work we consider mechanics of a precipitate growing in size as a result of a progressive phase transformation taking place at its boundaries. The phase transformation is assumed to occur in an infinitesimal layer at the boundary of the precipitate. An analytical solution is obtained for a homogeneous spherical geometry. The solution shows that stresses in the outer parts of the precipitate are compressive and closer to its centre stresses are tensile. A key feature of the solution is that the stresses become unbounded as the solution possess a logarithmic stress singularity at the centre of the sphere. Of course, in a real body, instead of a stress singularity the stress would be bounded at the expense of continuous material behaviour and would result in nucleation of cracks or voids.

A finite element model is verified against the exact solution. The model is then utilized to compute a crack growing in the centre of the growing precipitate. To simplify the treatment, the fracture toughness of the new phase is assumed to be insignificant. The assumption is not irrelevant considering that many precipitates are fragile and occasionally breaking at very low load, cf. Simpson and Cann (1979). Thus, a limit solution giving the largest possible self-grown crack is obtained under vanishing remote load. It should be pointed out that the difficulty in treating tougher materials lies in the selection of a proper fracture criterion and not in the subsequent numerical analyses.

2 The phase transformation

The precipitate studied here is supposed to grow as the result of a material flux from the surrounding body.
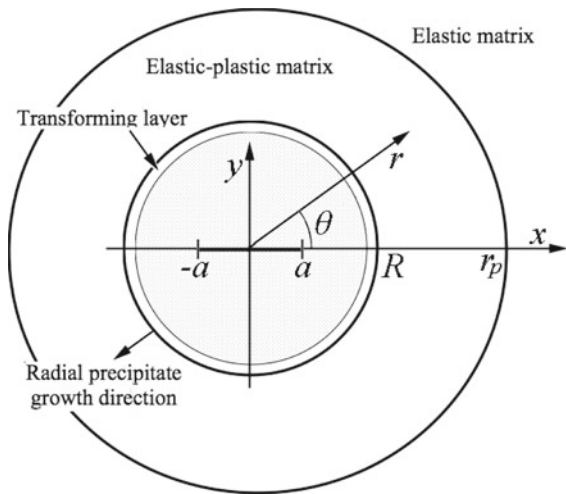
Fig. 2 Geometry of the growing precipitate. A spherical coordinate system is attached to the center of the precipitate. The precipitate-matrix boundary is at $r = R$ and the elastic plastic boundary in the matrix is at $r = r_p$. The phase transformation takes place in a thin layer at $r = R$. The *arrow* indicates that the boundary between the precipitate and the matrix is propagating in the radial direction

It is assumed that the flux is dilute and that the concentration is small so that the mechanical state of the body is unaffected by the material flux itself. As the transported matter accumulates at the surface of the precipitate the matrix material adjacent to the surface transform to the same phase as the precipitate material. Here this is treated as a continuous process. Thus, an infinitesimally thin layer of matrix material expands homogeneously in equal amounts in the directions normal and parallel to the surface (see Fig. 2). Due to the thinness of the layer the stress normal to the layer is expected to be constant during the transformation and further the strain in the directions along the layer is expected to be unaffected. In the latter case the reason is the constraint introduced by the surrounding material. Before the phase transformation, the material is loaded, possibly to the yield stress in tension. If the swelling strain is larger than twice the elastic strain limit, the mechanical state in the layer will first be elastic unloading and then reversely plastic when the yield stress is reached in compression in the direction parallel with the layer.

Because of this the maximum drop of elastic stress during the phase transformation is two times the yield stress, i.e., if the swelling strain is larger than two times the elastic strain limit the material will deform plastically during the phase transformation and become an

integral part of the precipitate that at least adjacent to the surface is at its yielding limit. This is in contrast to the solution by Eshelby (1957), Hill (1950) for which the stress state is constant and purely hydrostatic in the precipitate.

3 The model

Consider a solid sphere centred around the origin of a Cartesian coordinate system, x, y, and z. The sphere, with the radius R, is embedded in a large body. Further the sphere contains a penny-shaped crack with the radius c. A spherical coordinate system (r, θ, ψ) is attached to the centre of the sphere at $x = y = z = 0$. The spherical coordinates are defined as $r = \sqrt{x^2 + y^2 + z^2}$, $\theta = \arctan(y/x)$ and $\psi = \arccos(z/r)$. Figure 2 shows the geometry in the plane $z = 0$. The crack occupies the region $r < a$, $y = 0$. The sphere covers the region $r \leq R$. A surrounding matrix constitutes a large body, here regarded as infinite, i.e., it covers the remaining space $r > R$.

Both the sphere and the matrix are assumed to be elastic perfectly plastic with the modulus of elasticity E, Poisson's ratio ν and the yield stress σ_o. The yield criterion uses von Mises' effective stress, $\sigma_e = \sqrt{\sigma_r^2 + \sigma_\theta^2 + \sigma_\psi^2 + \tau_{r\theta}^2} \leq \sigma_o$.

The material of the sphere consists of transformed body material. The transformation of the body material takes place at the surface of the sphere. Thus, the sphere is growing by incorporating increasing amounts of transformed matrix material. As material is transformed it simultaneously undergoes a homogeneous swelling. This is modelled as an additional homogeneous strain, ε_s. The employed mathematical theory is based on assumed small strains. Thus, under stress free conditions, a volume V_e of body material would after the phase transformation occupy the volume $V_e(1 + 3\varepsilon_s)$.

The body is supposed to be subjected only to mechanical load caused by the expansion of the sphere. At large distances from the precipitate all stresses vanish. Displacements are assumed to remain finite everywhere. Because of the rotational symmetry there will not be any displacements in the ψ-direction and the derivative of any quantity with respect to this coordinate also vanishes. Therefore shear strains $\epsilon_{r\psi} = \epsilon_{\theta\psi} = 0$ and likewise the shear stresses $\sigma_{r\psi} = \sigma_{\theta\psi} = 0$.

The displacements u_r and u_θ define the following strains

$$\epsilon_r = \frac{\partial u_r}{\partial r}, \quad \epsilon_\theta = \frac{1}{r}\frac{\partial u_\theta}{\partial \theta} + \frac{u_r}{r}, \quad \text{and}$$

$$\epsilon_{r\theta} = \frac{\partial u_\theta}{\partial r} - \frac{u_\theta}{r} + \frac{1}{r}\frac{\partial u_r}{\partial \theta}. \tag{1}$$

The remaining non-zero strain component ϵ_ψ may be computed through a compatibility relation. Equilibrium requires

$$\frac{\partial \sigma_r}{\partial r} + \frac{1}{r}\frac{\partial \sigma_{r\theta}}{\partial \theta} + \frac{1}{r}(2\sigma_r - \sigma_\theta - \sigma_\psi + \sigma_{r\theta}\cot\theta) = 0. \tag{2}$$

and

$$\frac{\partial \sigma_{r\theta}}{\partial r} + \frac{1}{r}\frac{\partial \sigma_\theta}{\partial \theta} + \frac{1}{r}[(\sigma - \sigma_\psi)\cot\theta + 3\sigma_{r\theta}] = 0. \tag{3}$$

The strains are decomposed into elastic, plastic and swelling parts as follows

$$\epsilon_r = \epsilon_r^e + \epsilon_r^p + \epsilon^s,$$
$$\epsilon_\theta = \epsilon_\theta^e + \epsilon_\theta^p + \epsilon^s,$$
$$\epsilon_\psi = \epsilon_\psi^e + \epsilon_\psi^p + \epsilon^s \text{ and } \epsilon = \epsilon_{r\theta}^e + \epsilon_{r\theta}^p \tag{4}$$

where indices e, p and s denote the respective components.

The elastic strains are given by the stress using Hooke's law,

$$\epsilon_r^e = \frac{1}{E}\sigma_r - 2\frac{\nu}{E}\sigma_\theta, \quad \epsilon_\theta^e = \frac{1-\nu}{E}\sigma_\theta - \frac{\nu}{E}\sigma_r, \quad \text{and}$$

$$\epsilon_{r\theta}^e = \frac{1+\nu}{E}\sigma_{r\theta}. \tag{5}$$

The plastic strain components are proportional to deviatoric stresses as follows:

$$\frac{\epsilon_r^p}{\sigma_r - \sigma_h} = \frac{\epsilon_\theta^p}{\sigma_\theta - \sigma_h} = \frac{\epsilon_\psi^p}{\sigma_\psi - \sigma_h} = \frac{\epsilon_{r\theta}^p}{\sigma_{r\theta}}, \tag{6}$$

where σ_h is the hydrostatic stress defined as

$$\sigma_h = \frac{1}{3}(\sigma_r + \sigma_\theta + \sigma_\psi). \tag{7}$$

The relations Eqs. 6 and 7 readily lead to vanishing volumetric plastic strains. The Eqs. 1–7 are solved using the finite element code (ABAQUS 2007) for a body containing a crack. Without the crack the problem obtain spherical symmetry that simplifies the analysis. The following subsection is a derivation of the exact solution for this case.

3.1 Exact solution for a solid sphere

In the absence of a crack the problem provide spherical symmetry of load and geometry. Thus, the only remaining displacement is u_r. Because of that, all shear components vanish everywhere, and for obvious reasons $\epsilon_\theta = \epsilon_\psi$ and $\sigma_\theta = \sigma_\psi$. The strain components are given by

$$\epsilon_r = \frac{du_r}{dr} \quad \text{and } \epsilon_\theta = \frac{u_r}{r}. \tag{8}$$

The equations of equilibrium Eqs. 2 and 3 reduce to a single equation,

$$\frac{d\sigma_r}{dr} + 2\frac{\sigma_r - \sigma_\theta}{r} = 0, \tag{9}$$

cf. Hill (1950). It follows from Eqs. 6 and 7 that the sum of the plastic strain vanishes, i.e., $\epsilon_r^p + 2\epsilon_\theta^p = 0$. Using the notation $\epsilon^p = \epsilon_r^p$ inserted into Eq. 4, the following decomposition of strains is obtained

$$\epsilon_r = \epsilon_r^e + \epsilon^p + \epsilon^s, \quad \text{and} \quad \epsilon_\theta = \epsilon_\theta^e - \frac{1}{2}\epsilon^p + \epsilon^s. \tag{10}$$

The stress is given by

$$\epsilon_r = \frac{1}{E}\sigma_r - 2\frac{\nu}{E}\sigma_\theta + \epsilon^p + \epsilon^s,$$

$$\epsilon_\theta = \frac{1-\nu}{E}\sigma_\theta - \frac{\nu}{E}\sigma_r - \frac{1}{2}\epsilon^p + \epsilon^s. \tag{11}$$

After inserting Eqs. 11 and 8 into the equation of equilibrium Eq. 9 one obtains an ordinary differential equation for radial displacements as follows

$$\frac{d^2u_r}{dr^2} + 2\frac{du_r}{rdr} - 2\frac{u_r}{r^2} - \frac{1-2\nu}{1-\nu}\left(\frac{d\epsilon^p}{dr} + 3\frac{\epsilon^p}{r}\right) = 0 \tag{12}$$

Elastic matrix in $r > r_p$

For the elastic case, i.e., if the yield condition is not fulfilled $\epsilon_p = 0$ and while $\epsilon_s = 0$, the general solution of Eq. 12 is

$$u_r = C_1 r + C_2 r^{-2} \quad \text{in } r > r_p. \tag{13}$$

This solution is valid in the region remote from the precipitate. It is here assumed the yield criterion is met in the matrix at $r = r_p \geq R$. For the spherical symmetry, von Mises' yield condition gives $\sigma_o = \sigma_r - \sigma_\theta$, which then should be fulfilled at $r = r_p$. This and the condition that displacements should remain finite lead to

$C_1 = 0$ and $C_2 = \frac{1+\nu}{3}\frac{\sigma_o r_p^3}{E}$.

Elastic-plastic matrix in $R < r \leq r_p$

For the plastic solution when the yield condition is fulfilled, then $\sigma_r - \sigma_\theta = \sigma_o$ and the equation of equilibrium Eq. 9 becomes

$$\frac{d\sigma_r}{dr} + 2\frac{\sigma_o}{r} = 0, \tag{14}$$

The general solution can be written

$$\sigma_r = C_3 + 2\sigma_o \ln\frac{r}{r_p}. \tag{15}$$

Continuous radial stress at $r = r_p$ gives $C_3 = -\frac{2}{3}\sigma_o$. This inserted into Eqs. 11 and 10 requires continuity also for the plastic strain, i.e., that $\epsilon_p = 0$ as $r \to r_p$ in $r < r_p$. The displacements are found by inserting Eq. 19 into Eq. 11, using the compatibility relation between ϵ_r and ϵ_θ, Eq. 8. This, leads to the following solution for the plastic strain

$$\epsilon^p = \frac{2(1-\nu)\sigma_o}{E}\left[1 - \left(\frac{r_p}{r}\right)^3\right]. \tag{16}$$

Using the radial stress from Eq. 15 and tangential stress obtained from the yield condition and the plastic strain according to Eq. 16 allow calculation of the displacements using Eq. 10. The result becomes

$$u_r = \left[(1-\nu)\left(\frac{r_p}{r}\right)^3 - \frac{2(1-2\nu)}{3}\left(1-3\ln\frac{r}{r_p}\right)\right]\frac{r\sigma_o}{E}$$
$$\text{in } R < r \leq r_p. \tag{17}$$

In the elastic-plastic region $r > R$ the solution coincide with Hill's (1950) solution. However, in the precipitate the solutions differ due to the mechanics of expansion leading to plastic deformation. Here the progressive expansion of matrix material takes place at the surface of the precipitate. In the model the thickness of the layer undergoing expansion is considered to be infinitesimal.

Elastic-plastic precipitate in $r \leq R$

Provided that the swelling is sufficient to produce reversed plastic deformation in the transformed layer, then $\sigma_r - \sigma_\theta = -\sigma_o$ and, thus, the equation of equilibrium becomes

$$\frac{d\sigma_r}{dr} - 2\frac{\sigma_o}{r} = 0, \tag{18}$$

with the general solution

$$\sigma_r = C_4 - 2\sigma_o \ln\frac{r}{R}. \tag{19}$$

Continuity conditions require that radial stress and displacement should be continuous across $r = R$. However, continuous plastic strains are not needed because of the arbitrary swelling ϵ_s occurring at $r = R$. Instead the condition that the displacements vanish at $r = 0$ is added to the equations. Continuous radial stress at $r = R$ gives $C_4 = \left[-\frac{2}{3} + 2\ln\left(\frac{R}{r_p}\right)\right]\sigma_o$. The compatibility of strains requires a constant plastic strain and for the displacements to be continuous at $r = R$, the plastic strain have to be $\epsilon^p = -2(1-\nu)(\sigma_o/E)$. The resulting displacements are

$$u_r = \epsilon_s r - \frac{2(1-2\nu)}{3}\left(1 + 3\ln\frac{r_p r}{R^2}\right)\frac{\sigma_o r}{E} \quad \text{in } r \leq R. \tag{20}$$

The displacements of Eqs. 17 and 20 do generally not coincide as $r \to R$. A condition for this is readily obtained as a specification of r_p as follows,

$$r_p = R\sqrt[3]{\frac{E\epsilon_s}{2(1-\nu)\sigma_o}}. \tag{21}$$

Equation 21 also provide a lower limit for the swelling while $r_p \geq R$. The lower limit is denoted ϵ_o defined as

$$\epsilon_s \geq \epsilon_o = \frac{2(1-\nu)\sigma_o}{E}. \tag{22}$$

Should the swelling be less than ϵ_s strain material does not yield in the matrix. As a coincidence then the swelling during expansion does not either produce reversed plasticity meaning that the suggested solution does not apply. As being purely elastic the solution Eshelby (1957) should apply to this case. Equations 20, 17 and 13 give the exact solution in the regions $r \leq R$, $R < r \leq r_p$ and $r_p < r$, respectively.

4 Modelling of a crack

The finite-element computations have been performed using the ABAQUS (2007) computer program. ABAQUS offers the possibility to adding increasing swelling using an analogous heat expansion. The constitutive law described in the preceding section has been implemented in ABAQUS invoking a two-dimensional axisymmetric solid material element. In the model eight-node isoparametric element, with two nodal degrees of freedom, in a cylindrical polar coordinate system is utilized. Reduced integration with evaluation at four Gaussian points is used.

A quarter circle $r \leq 10R$, $0 \leq \theta \leq \pi$ is covered by 10,000 elements each occupying a radial interval $\Delta r = 0.02R$ and an angular region $\Delta \theta = 4.5°$. Through the axisymmetry of the elements the upper half-sphere is covered and symmetry boundary conditions in the plane $a < r \leq 10R$, $\theta = 0$ and traction free boundaries at $r \leq a$, $\theta = 0$. The size of the modelled sphere is believed to be sufficiently large to accurately behave as a very large body.

5 Results

The calculations are made using dimensionless variables. Here stress, strain and displacement components are scaled with σ_o, σ_o/E and $R\sigma_o/E$, respectively. The only significant material parameters are Poisson's ratio, ν, and the swelling strain ϵ_s. The former is put to 0.3 and the latter is, for the exact solutions, selected to be 1, 4.5, 8, 11.5 and 15 times ϵ_o, where $\epsilon_o = 2(1 - \nu)$ σ_o/E. With a crack present numerical calculations are made for $\epsilon_s = 8\epsilon_o$.

Displacements in the radial direction, according to Eqs. 20, 17 and 13, are plotted in Fig. 3. As observed displacements increase from zero at $r = 0$ to a maximum value at generally at $r = R$. However, for small swelling maximum displacements occur in the interior of the precipitate, e.g., for $\epsilon_s = \epsilon_o$ maximum is obtained at $r = \exp\{(13\nu\text{-}5/)/[6(1 - 2\nu)]\}$. For the selected Poisson's ratio maximum displacement occurs at $r = 0.632R$. The dot-dashed straight line indicate at its crossing with the displacement curves, the position of the corresponding elastic-plastic boundary $r = r_p$ in the matrix.

The dashed curves in Fig. 3 are the finite element results for $\epsilon_s = 8\epsilon_o$ giving $r_p \approx 2R$. The deviation from the exact solution is, as observed, very small. The solid curve for the exact result is, almost to invisibility, covered by the dashed curve for the finite element result. Also the discontinuous tangential stress, including the discontinuity at $r = R$, is accurately represented by the finite element result. The result is in great contrast to Hill's (1950) solution as regards the stresses in the precipitate. The most significant difference is that both the radial stress and the tangential stress are tensile stresses in the centre of the precipitate. From Eq. 19 one finds that the radial stress is tensile in the region $r < \frac{R}{r_p} \exp\left(-\frac{1}{3}\right) R$. For the case $\epsilon_s = 8\epsilon_o$ giving $r_p = 2R$ one get tensile radial stress
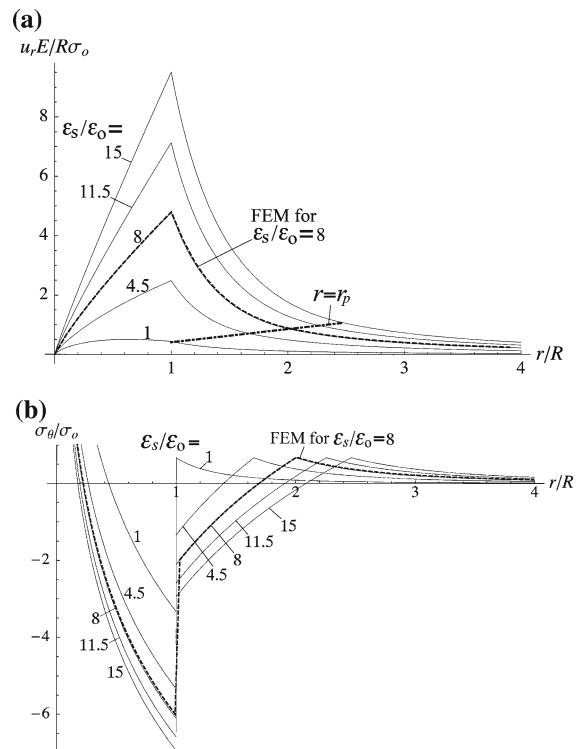
(a)

(b)

Fig. 3 **a** Radial displacements and **b** tangential stress for $\epsilon_s/\epsilon_o = 2$, 4.5, 8, 11.5 and 15. The dashed curves are FEM results for $\epsilon_s = 8\epsilon_o$. In all cases $\nu = 0.3$. The *dot-dashed straight line* show the extent of the plastic zone in the matrix, i.e., for larger distances from the centre of the precipitate the material is elastic

for $r \lesssim 0.358R$. The tangential stress is tensile in the region $r < \frac{R}{r_p} \exp\left(-\frac{5}{6}\right) R$. For $\epsilon_s = 8\epsilon_o$ one get tensile tangential stress for $r \lesssim 0.217R$. According to the finite element result the tangential stress is tensile for $r \lesssim 0.22R$.

Figure 4 shows the half-length a of the growing crack as a function of the radius, R, of the precipitate. The problem is self-similar and R should be the only length scale. The final radius of the precipitate is covered by 50 elements. All elements have the same length l in the radial direction. Any deviation from a linear relation between crack length and precipitate radius should be due to interference with the numerical length scale introduced by either the element size l or the radius, $10R = 500l$, of the finite meshed body. As observed in the plot, the result is remarkably independent of the precipitate versus element length ratio. A small deviation is observed when the precipitates has grown above $R = 40l$. The linear relation between
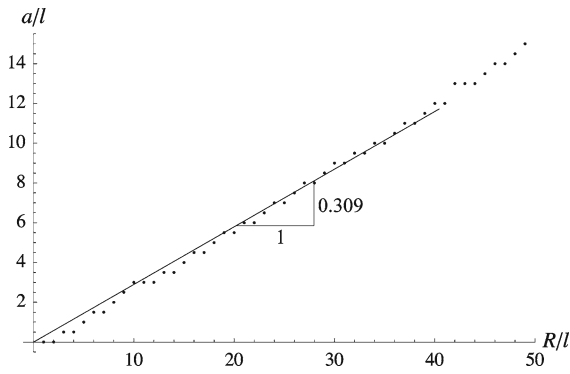
Fig. 4 Half-length a of the growing crack as a function of the linear extent, R, of the precipitate. The problem is self similar and R should be the only length scale. The final radius of the precipitate is covered by 50 elements. All elements have the same length l along the radial axis

half-length a of the crack and the precipitate radius R determined from this diagram is $a = 0.309R$ element size. The result is obtained as a least square fitting of a straight line $a = kR$ after excluding precipitates larger than $40l$.

The crack opening displacement u_θ along $0 < r \leq a$, $\theta = 0$ is shown in Fig. 5 shows the crack opening displacement. Because of the assumed insignificant crack tip load the crack surface displacement is smooth at $r = a$. Maximum displacement is assumed to occur at the centre of the crack, at $r = 0$. The dip observed in the vicinity only involves one element and is observed to do that during the entire growth history. Therefore, this dip is assumed to be a numerical artefact. How well the numerically obtained displacements reflect the character of the model remain an unresolved question. The relaxed stresses as obtained from the case, without the crack present, possess a logarithmic singularity that would if the unloading is elastic, not lead to unbounded displacements. However, these speculations seem to have little practical significance.

In Fig. 6 the radial displacements, u_r, and tangential stress, σ_θ, are compared with the respective exact results without a crack. Very small differences are observed. The presence of the crack decreases the radial displacements in the crack plane, but only around 0.5%. The displacements perpendicular to the crack plane increase around 1%. The tangential stress seemingly only change in the neighbourhood of the crack. The effect of the crack on the stress in the matrix seems to be marginal.
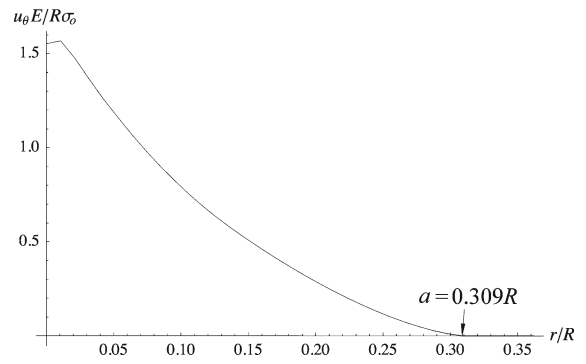

Fig. 5 Crack opening displacements, u_θ for $R = 50l$
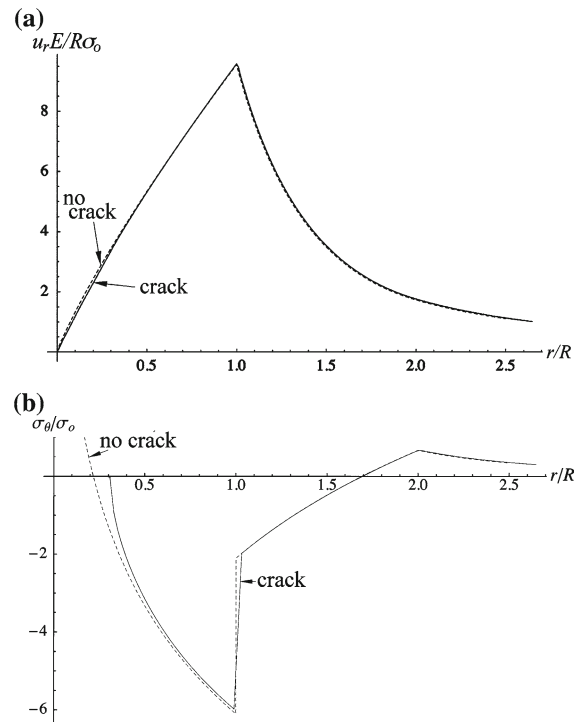

Fig. 6 **a** Radial displacements and **b** tangential stress for $\epsilon_s = 8\epsilon_o$, along $\theta = 0$. The *dashed curves* are exact results and the *solid curves* are FEM results for the geometry containing a crack woth the half-length $a = 0.309R$

The hydrostatic stress $\sigma_h = \sigma_r + \sigma_\theta + \sigma_\psi$ is plotted in Fig. 7 in a quarter of a cut through the precipitate. Because of the rotational symmetry and the symmetry across the x, y-plane, the plot represents the region $|x| \lesssim 1.3R$, $|y| \lesssim 1.3R$ and $|z| \lesssim 1.1R$. The hydrostatic stress is practically constant in the region $r \gtrsim r_p$ and then decreasing as r approaches R. Inside the precipitate the hydrostatic stress increases
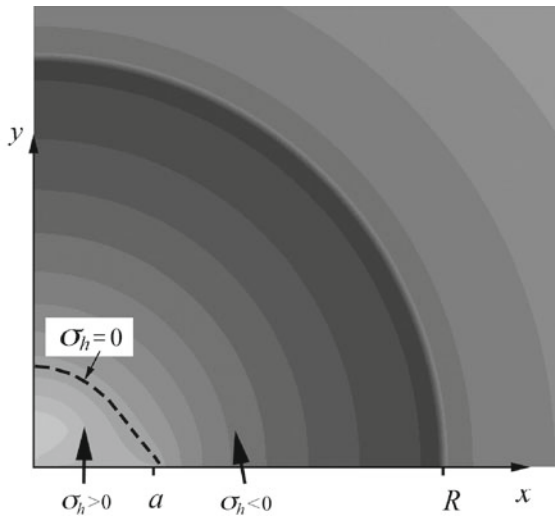
Fig. 7 Hydrostatic stress distribution for $\epsilon_s/\epsilon_o = 8$. FEM results in the region $0 \leq x \lesssim 1.3R$, $y = 0$ and $0 \leq z \lesssim 1.1R$

with decreasing r. The curve across which the hydrostatic stress becomes positive is marked in the plot.

6 Discussion

Brittle precipitates cause problems in industrial applications because of the risk of fracture. One obvious risk is a self-cracked precipitate that may be the initiation point of fatigue or rapidly growing cracks when tensile load is applied.

The stress distribution of the present solution is in significant contrast to previous solutions for expanding inclusions. The singular stresses in the centre of the precipitate according to the model will in the real case lead to non-linear material behaviour. Considering the stress state as hydrostatic the most probable result would be initiation of voids or micro-cracks.

In the present context the stress distribution in the precipitate represents the most dramatic change as compared with simultaneous swelling of the entire precipitate. The primary source of the differences is the incremental growth of the precipitate, where the material is swelling in an thin layer at the surface of the precipitate, thus progressively increasing the area covered by the precipitate. The mechanism that for each added layer leads to an increment of tensile hydrostatic stress in the precipitate develop a singular stress singularity at the centre of the precipitate. The solution is found for spherical precipitates. If one should

speculate in what the result would be for a non-spherical precipitate, considering the mechanism the obvious suggestion would be that any self-similar growing precipitate would develop a singularity at the position where the precipitate was nucleated. Thus, also micro-cracks are expected for virtually arbitrary shaped precipitates. Even surface precipitates, so called blisters, ought to be included. This is supported also by observations (Singh 2009).

The fact that the stress state is little influenced by the presence of the crack may be connected to the investigated geometry, e.g., an oblate elliptic precipitate would probably be more sensitive to the presence of the crack, thus, exerting larger compressive load on the matrix in the regions above and below the crack plane. This may be important since the shape of precipitates that often form ahead of crack tips, thus causing so called delayed hydride cracking are observed to be elliptic, and may thus require the present model to get a correct picture of the mechanical state even in the matrix.

The mathematical analysis suggests that cylindrical precipitates could easily be incorporated, whereas the plastic deformation is constant inside the precipitate, thus also hardening materials should be straightforward to analyse. The part that needs to be derived is the deformation of the matrix.

7 Conclusions

The stress state of a growing precipitate with misfit strain is calculated modelling the phase transformation after incremental expansion of the precipitate. In an intact precipitate with spherical shape the stress possess a logarithmic stress singularity at the centre of the precipitate. The stresses in the centre of the precipitate are tensile and essentially hydrostatic. The effective stress remains constant everywhere inside the precipitate at the yield stress. In surrounding matrix for large misfit strain there is a plastic region adjacent to the precipitate and further out the material is elastic with magnitudes of stress decaying with increasing distance.

A growing crack is studied for a case with insignificant material toughness. The crack criterion is vanishing tensile stress ahead of the crack tip. The crack is observed to cover around a third of the precipitate diameter. The result finds support in observed star shaped micro-crack in precipitates grown in an experiment.

Because of the absence of tensile stress in the outer parts of the precipitate the crack remain embedded on the precipitate and long as no remote load is present. Under self-similar growth of a spherical precipitate up to around 40% of the linear extent of the precipitate is under tensile tangential stress and up to 70% is under tensile radial stress.

While the mechanical state of the precipitate is totally changed, in the matrix it is identical and not affected of if the precipitate swelling is incremental or occurring simultaneously in the entire precipitate when the precipitate is intact. When a crack is present the stresses and displacements in the matrix are altered but only around at most a percent.

References

ABAQUS (2007) User's manual. HKS, Providence

Eshelby JD (1957) The determination of the elastic field of an ellipsoidal inclusion, and related problems. Proc R Soc Lond Ser A Math Phys Sci 241:376–396

Grange M, Besson J, Andrieu E (2000) An anisotropic Gurson type model to represent the ductile rupture of hydrided Zircaloy-4 sheets. Int J Fract 105:273–293

Hill R, Lee EH, Tupper SJ (1947) The theory of combined plastic and elastic deformation with particular reference to a thick tube under internal pressure. Proc R Soc Lond Ser A Math Phys Sci 191(1026):278–303

Hill R (1950) The mathematical theory of plasticity. Clarendon Press, Oxford

Leitch BW, Puls MP (1992) Finite element calculation of the accommodation energy of a misfitting precipitate in an elastic-plastic matrix. Metall Trans 23A:797

Leitch BW, Shi S-Q (1996) Accommodation energy of formation and dissolution for a misfitting precipitate in an elastic-plastic matrix. Model Simul Mater Sci Eng 4:281–292

Matvienko YG (2004) The cohesive zone model in a problem of delayed hydride cracking of zirconium alloys. Int J Fract 128:73–79

Puls MP (1984) Hydrogen-induced cracking: 2 effect of stress on nucleation, growth and coarsening of Zirconium hydride precipitates. Atomic Energy of Canada Ltd. Report No AECL-8381

Puls MP (1990) Effect of crack tip stress states and hydride matrix interaction stresses on delayed hydride cracking. Metall Trans A, 21A

Shi S-Q (1999) Diffusion-controlled hydride growth near crack tip in zirconium under temperature transients. J Nucl Mater 275:318–323

Simpson LA, Cann CD (1979) Fracture toughness of zirconium hydride and its influence on the crack resistance of Zirconium alloys. J Nucl Mater 87:303–316

Singh RN, Ståhle P (2006) Fracture of Zr-alloy pressure tubes due to hydride blister formation. In: Presented at 19th Nordic seminar in computational mechanics—NSCM19 hosted by Lund University, Faculty of Engineering on 20–21 Oct 2006, Lund, Sweden

Singh RN, Ståhle P, Banks-Sills L, Ristmanaa M, Banerjee S (2008a) δ-hydride habit plane determination in α-Zirconium at 298 K by strain energy minimization technique. Defect Diffus Forum 279:105–110

Singh, RN, Ståhle P, Sairam K, Chakravartty JK, Kashyap BP (2008b) Stress-field Computation for hydride blister forming in Zr-alloys. Water reactor fuel performance meeting—WRFPM2008 Seoul, South Korea 19–23 Oct 2008, paper No 8137

Singh RN, Kishore R, Singh SS et al (2004) Stress-reorientation of hydrides and hydride embrittlement of Zr–2.5 wt% Nb pressure tube alloy. J Nucl Mater 325:26–33

Singh RN (2009) Private communication

Taylor GI (1948) The formation and enlargement of a circular hole in a thin plastic sheet. Q J Mech Appl Math 1:103–124